Kalman Filter based robust GNSS signal tracking algorithm in presence of ionospheric scintillations

Valentin Barreau, Willy Vigneau, Christophe Macabiau, Lina Deambrogio

Kalman Filter Based Robust GNSS Signal Tracking Algorithm in Presence of Ionospheric Scintillations

Valentin BARREAU, Willy VIGNEAU
M3SYSTEMS
Toulouse, France

Christophe MACABIAU, Lina DEAMBROGIO
ENAC/Université de Toulouse
Toulouse, France

Ionospheric scintillations are created by diffraction when the transmitted propagating waves encounter a medium made of irregular structures with variable refraction indexes. The recombination of the waves after propagation can be constructive or destructive and the resulting signal at output of the receiver antenna may present rapid variations of phase and amplitude.

The carrier phase is traditionally tracked in the GNSS receivers using PLL, potentially aided by FLL. Phase Loops are known to be less robust than code tracking loops, and the GNSS receivers may thus suffer from phase tracking loss. This strongly impacts the positioning service availability, as well as the capability to demodulate the navigation message data, in situations where ionospheric scintillations affect the received signal. One thus has to implement innovative techniques and receiver architectures to provide robust carrier phase tracking.

The aim of this paper is therefore to present the development of a GPS L1 phase tracking technique based on a Kalman Filter PLL [10] improving the tracking robustness in presence of ionospheric scintillations, and to present results of its performance using simulations. This paper is related to the paper presented at ION GNSS 2012 by C. Macabiau [1].

Kalman filter; scintillation; GISM; robust tracking loop

I. INTRODUCTION

Scintillation is a well-known phenomenon when observing stars in a summer night, imaging amplitude and phase fluctuations of electromagnetic waves. The cause can be diffraction when the waves cross a medium composed of irregular structures with variable refraction indexes.

Ionospheric scintillations concern signal fluctuations in VHF and UHF radio band up to C band which propagate through the ionized atmospheric layer between 100 and 1000 km, but most particularly in the F2 layer between 250 and 600 km, when it is affected by heterogeneities. The intensity of the effects depends on the signal frequency compared to the plasma frequency and the level of irregularity.

Several studies showed a dependency on the solar cycle, as the maximum observed intensities coincide with the maximum UV radiated by the sun and the maximum electronic density in the ionosphere [3].

The physical phenomena that lead to scintillation effects are not well understood yet and are the subject of researches.
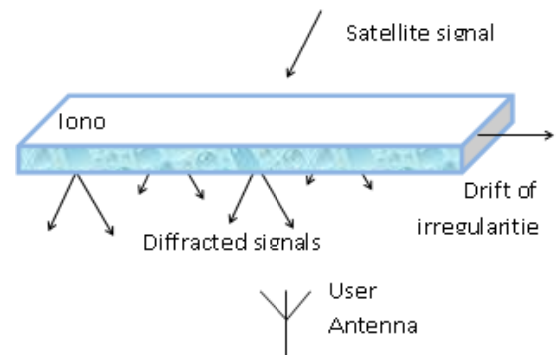

Figure 1: Illustration of ionospheric drift of irregularities leading to ionospheric scintillations.

II. BACKGROUND AND SIGNAL MODEL

A. Different types of scintillations phenomena

1) Equatorial scintillations

In the ionospheric plasma, bubbles with weak ionization level appear frequently after sunset in the lower part of the ionosphere (typically at altitudes between 200 and 400 km) then go up at higher altitudes [8]. Observations in America, Africa and India reveal the occurrence of peaks at the equinoxes and the quasi total absence of scintillations during summer. In Pacific, the seasonal influence is inversed with observed maxima from April to August [4].

2) High latitude scintillations

We distinguish the region of the polar cornet in which the magnetic field lines are open to the solar wind and the auroral oval, band centered on the geomagnetic pole between 60 and 75 degrees of latitude.

Practically, the polar cornet is an open magnetic region where phase and amplitude scintillations can happen. The auroral oval is a magnetic region where lines are closed, phase scintillations are predominant. High latitude scintillations are more intense in winter when the solar radiations do not smooth the ionization irregularities.

3) Mid-latitude scintillations

After an intense magnetic storm and in particular if its origin is a solar eruption with energetic particles, e.g. during coronal mass ejection, the engendered ionospheric perturbation can migrate towards the south.

B. Effects on GNSS signals

The ionosphere causes a group delay of the modulation and a phase advance. Ionosphere irregularities that cause GNSS scintillations can affect the GNSS signal through refraction and diffraction causing rapid variations of the group delay and phase shift of the carrier [6] as well as strong amplitude attenuations of the signal.

The combination of these phenomena disturbs the lock on the carrier, generating bit errors, cycle slips and even complete loss of the signal tracking. The consequences on GNSS systems are the loss of continuity of service, degradation of accuracy and loss of integrity.

C. Scintillations modelling with GISM

1) Model description

The GISM model (Global Ionospheric Scintillation Model) enables to compute the scintillation effects on a signal after the crossing of the ionosphere between a fixed terrestrial receiver and a GPS satellite. It is a climatological model, in which statistical properties are associated to the medium to take into account the known characteristics of its spectrum, the effect of the solar cycle and of local time. It uses the MPS technique (Multiple Phase Screen) to solve the wave propagation equations and to determine the expected fluctuations. The medium is divided in successive layers, each acting as a phase screen. The line of sight is first computed considering the different indices of the layers crossed and thus the incident and refracted angles. Then the electron density is given by the model at each layer by the NeQuick model [11]. The fluctuations and the generated errors are computed by solving the Haselgrove equations. The signal spectrum is characterized by 3 parameters: the slope, the cut-off frequency and the lowest frequency. The slope is comprised between -2 and -3. A detailed model is given in [2].

The model inputs are:
- The date of the simulations
- The solar flux
- The geographical coordinates at the observation point

The main outputs of the model are:
- The time series of the amplitude and phase of the signal at the selected frequency.
- The estimated S4 and sigma-phi computed every minute.

2) Model limitations

The model described above is only applicable in the equatorial region. The phase screen model is insufficient because a distinction is needed between the 2 affected regions, the polar cornet and the auroral oval, each with different mechanisms.

Another limitation of the scintillation model is that it does not reflect reality, which is the presence of low electron density irregularities concentrated in space but a medium with layers with identical characteristics at a given time all around the observation point. Thus, there is no representativeness of the fraction of the satellite constellation affected by the phenomenon; all satellites are affected in a homogeneous way.

III. REVIEW OF SCINTILLATION TRACKING TECHNIQUES

In this section, only the techniques at signal processing level will be considered.

The aim of the techniques will be to improve the robustness of the carrier phase tracking, in order to increase the capability of the loops to follow accurately the phase variations; the objective will be to decrease the number of phase tracking losses and to limit the impact on the provided measurements (including data demodulation).

A. Conventionnal loops

Conventional PLL (Phase Lock Loop) are based on closed loop filtering of phase discriminator to perform signal tracking. Those conventional architectures have limited performance for tracking carrier phase in difficult conditions. However, the fine tuning of the loops parameters may increase the robustness of carrier phase tracking but a trade-off is still to be done between accuracy and robustness.

B. Adaptative Loop Bandwidth

On top of the classical loops, "Fast Adaptive Bandwidth" (FAB) technique [9] has been developed to minimize the total tracking error in presence of noise or dynamics. For high dynamics, FAB works to increase loop bandwidth and to decrease it in case of noise.

But FAB is not really effective during scintillation [7] because the C/N0 can be very low and at the same time as the phase variations can be very fast.

C. Kalman filter-based tracking loop

Kalman loop filter provides in theory the optimal filter gain when the statistical level of noise of the inputs is well known.
Two options can be considered:
- A 3-state (phase error, Doppler frequency, and Doppler frequency rate) 2-equations (prediction and update) Kalman filter is typically used with a constant gain [10]. KFP allows better performances compared to conventional tracking [16].
- A classical 5-equations Kalman filter (including the prediction steps) which would require state noise and observation noise knowledge, which is usually difficult to obtain. Moreover, the lack of knowledge about the equivalent loop bandwidth may cause some problems in case of phase tracking integrity monitoring.

D. Vectorized architecture

Vectorized architecture merges observations from all the channels to use most of the available useful information while averaging the tracking errors on each channel and to improve robustness of tracking with aid of all the individual channels tracking [5].

This kind of architecture allows reducing the impact of jamming and interferences, allows tracking at lower C/N0, and offers a greater immunity to receiver's dynamic. Moreover, in

case of signal outage on one of the channels, the receiver keeps following signal dynamic and so allows the tracking to restart as soon as sufficient signal power comes back.

But as soon as the position estimate is wrong, the position error will be introduced in all the tracking channels and eventually could cause the loss of all the channels. Moreover, vectorized phase tracking would require only very small position errors to be performed.

E. Other techniques

Other techniques can be used, inherited from other domains such as telecommunication:

- Wavelet de-noising techniques can help to reduce the noise on tracking channels, based on wavelet transform algorithms [13]. The results shown by this technique are interesting in terms of performance but the processing load and complexity is rather high and real time implementation may be compromised.

- Open loop architectures [14] have the advantages to be more robust than a closed loop filter since the output is not fed back on the entry of the filter (the errors cannot propagate epoch-to-epoch). The major drawback is the large complexity of the receiver.

IV.   ANALYSIS OF KALMAN FILTER TRACKING TECHNIQUES

A. Kalman filter description

The KFP algorithm (Kalman Filter Phase lock loop) is based on the models and assumptions presented in [10]. This algorithm enables to implement a carrier tracking loop of order 3.

The signal processed by the receiver is the GPS L1 C/A signal. The duration of one bit of the navigation message is thus 20ms. Let us denote t_k the time at which the correlator outputs are provided. We define $\Delta t_k = t_{k+1} - t_k$ the duration of the coherent integrations. We define K the number of correlator outputs available within the duration of one bit of the navigation message. We define I_k and Q_k the correlator outputs available at time t_k, i.e. the correlator outputs computed during the interval $t_{k-1} \dots t_k$.

We define ω_{PLLk} the value of the NCO control signal during the interval $t_k \dots t_{k+1}$. The phase of the PLL NCO is computed as $\phi_{PLL}(k+1) = \phi_{PLL}(k) + \Delta t_k \omega_{PLLk}$.

We define $X_k = \begin{bmatrix} \Delta\phi_k \\ \omega_k \\ \alpha_k \end{bmatrix}$ the state vector of the Kalman Filter,

with

- $\Delta\phi_k$ the difference between the phase of the incoming carrier and the phase of the local carrier generated by the NCO

- ω_k the difference between the doppler shift of the incoming carrier and the Doppler shift of the local carrier generated by the NCO in rad/s (pulsation)

- α_k the difference between the jerk of the incoming carrier and the jerk of the local carrier generated by the NCO

This algorithm only includes 2 equations of the Kalman Filter among the 5 traditional equations. Indeed, the Kalman gain K is proposed to be fixed, therefore the two covariance equations, during the prediction and update, are useless and are not considered. It also includes an iterative algorithm allowing deciding the value of the bit of the navigation message affecting the correlator outputs I_{k+1} et Q_{k+1} in order to provide the extended arctangent discriminator outputs. The 2 equations of the Kalman Filter to be run every t_{k+1} are:

$$\begin{bmatrix} \Delta\hat{\phi}_{k+1|k} \\ \hat{\omega}_{k+1|k} \\ \hat{\alpha}_{k+1|k} \end{bmatrix} = \begin{bmatrix} 1 & \Delta t_k & 0.5\Delta t_k^2 \\ 0 & 1 & \Delta t_k \\ 0 & 0 & 1 \end{bmatrix} \begin{bmatrix} \Delta\hat{\phi}_{k|k} \\ \hat{\omega}_{k|k} \\ \hat{\alpha}_{k|k} \end{bmatrix} + \begin{bmatrix} -\Delta t_k \\ 0 \\ 0 \end{bmatrix} \omega_{PLLk}$$

$$\begin{bmatrix} \Delta\hat{\phi}_{k+1|k+1} \\ \hat{\omega}_{k+1|k+1} \\ \hat{\alpha}_{k+1|k+1} \end{bmatrix} = \begin{bmatrix} \Delta\hat{\phi}_{k+1|k} \\ \hat{\omega}_{k+1|k} \\ \hat{\alpha}_{k+1|k} \end{bmatrix} + K \left[\nu_{k+1} - 2\pi \times \text{round}\left(\frac{\nu_{k+1}}{2\pi}\right) \right]$$

The authors of [10] propose that the Kalman gain K is not updated, but considered fixed and defined such that the matrix $\begin{bmatrix} 1 & \Delta t_k & 0.5\Delta t_k^2 \\ 0 & 1 & \Delta t_k \\ 0 & 0 & 1 \end{bmatrix} - K \begin{bmatrix} 1 & \frac{\Delta t_k}{2} & \frac{\Delta t_k^2}{6} \end{bmatrix}$ has the eigenvector $\begin{bmatrix} e^{-2\pi B_{PLL}\Delta t_k} \\ e^{[-1+i\sqrt{3}]\pi B_{PLL}\Delta t_k} \\ e^{[-1-i\sqrt{3}]\pi B_{PLL}\Delta t_k} \end{bmatrix}$.

We obtain the values of the gain K, as a function of the desired loop bandwidth and integration time:

- For B_{PLL}=2.5 Hz and Δt_k=10 ms,
$$K = \begin{bmatrix} 0.291004 \\ 4.391752 \\ 33.123850 \end{bmatrix}$$

- For B_{PLL}=10 Hz,

    o and Δt_k = 1 ms, $\quad K = \begin{bmatrix} 0.121817 \\ 7.533759 \\ 232.944295 \end{bmatrix}$

    o and Δt_k = 10 ms, $\quad K = \begin{bmatrix} 0.943983 \\ 50.129594 \\ 1323.319695 \end{bmatrix}$

    o and Δt_k = 20 ms, $\quad K = \begin{bmatrix} 1.475514 \\ 65.065271 \\ 1412.041091 \end{bmatrix}$

The innovation considered is $\nu_{k+1} = y_{k+1} - \hat{y}_{k+1|k}$.

The measurement prediction is:

$$\hat{y}_{k+1|k} = \begin{bmatrix} 1 & \frac{\Delta t_k}{2} & \frac{\Delta t_k^2}{6} \end{bmatrix} \begin{bmatrix} \Delta\hat{\phi}_{k+1|k} \\ \hat{\omega}_{k+1|k} \\ \hat{\alpha}_{k+1|k} \end{bmatrix} - \frac{\Delta t_k}{2} \omega_{PLLk}.$$

The considered measurement vector is computed from the discriminator output. If we want to use an ATAN2

discriminator, it is necessary to estimate the value of the data bit. In this case, the measurement is obtained as:

$$y_{k+1} = \text{atan2}\left(\hat{d}_{bit(k+1|k)}Q_{k+1}, \hat{d}_{bit(k+1|k)}I_{k+1}\right).$$

This discriminator output uses a prediction of the value of the bit of the navigation message under the form:

$$\hat{d}^1_{bit(k+1|k)}$$
$$= \begin{cases} +1 \text{ if } I_{bit(k+1)}\hat{I}_{bit(k+1|k)} + Q_{bit(k+1)}\hat{Q}_{bit(k+1|k)} \geq 0 \\ -1 \text{ if } I_{bit(k+1)}\hat{I}_{bit(k+1|k)} + Q_{bit(k+1)}\hat{Q}_{bit(k+1|k)} < 0 \end{cases}$$

$$I_{bit(k+1)} = \sum_{i=K\text{floor}\left(\frac{(k+1)}{K}\right)}^{(k+1)} I_i,$$

$$Q_{bit(k+1)} = \sum_{i=K\text{floor}\left(\frac{(k+1)}{K}\right)}^{(k+1)} Q_i$$

And
$$\hat{I}_{bit(k+1|k)} = \sum_{i=K\text{floor}\left(\frac{(k+1)}{K}\right)}^{(k+1)} \cos(\hat{y}_{i|i-1}),$$

$$\hat{Q}_{bit(k+1|k)} = -\sum_{i=K\text{floor}\left(\frac{(k+1)}{K}\right)}^{(k+1)} \sin(\hat{y}_{i|i-1})$$

Note that we can envisage another technique of prediction of the navigation message bits which is:

$$\hat{d}^2_{bit(k+1|k)} =$$
$$\begin{cases} +1 \text{ si } \sum_{i=K\text{floor}\left(\frac{(k+1)}{K}\right)}^{(k+1)} \left[I_i\cos(\hat{y}_{i|i-1}) - Q_i\sin(\hat{y}_{i|i-1})\right] \geq 0 \\ -1 \text{ si } \sum_{i=K\text{floor}\left(\frac{(k+1)}{K}\right)}^{(k+1)} \left[I_i\cos(\hat{y}_{i|i-1}) - Q_i\sin(\hat{y}_{i|i-1})\right] < 0 \end{cases}$$

If the measurement uses the output of an atan discriminator, the estimation of the data bit is then useless and the measurement is directly $y_{k+1} = \text{atan}\left(\frac{Q_{k+1}}{I_{k+1}}\right)$.

Note that the authors of [10] propose to compute the NCO control signal ω_{PLLk} in the following way:

$$\omega^1_{PLL(k+1)} = \frac{1}{\Delta t_{k+1}}\left[(1-\eta)^2\left(\Delta\hat{\phi}_{k|k} - \Delta\phi_{des}\right) \right.$$
$$\left. + (1-2\eta)\Delta t_k\left(\hat{\omega}_{k|k} - \omega_{PLLk}\right) - \eta\Delta t_k^2\hat{\alpha}_{k|k}\right]$$
$$+ \hat{\omega}_{k|k} + \frac{(\Delta t_k + \Delta t_{k+1})^2}{2\Delta t_{k+1}}\hat{\alpha}_{k|k}$$

Where:

- $\Delta\phi_{des}$ is such as $\Delta\hat{\phi}_{k+2|k+2} - 2\,\eta\Delta\hat{\phi}_{k+1|k+1} + \eta^2\Delta\hat{\phi}_{k|k} = (1-\eta)^2\Delta\phi_{des}$

- η is a tuning factor that can be chosen such as $\eta = 0.774597$, or very close to 1 if we want to limit the velocity of convergence of $\Delta\phi_k$ towards $\Delta\phi_{des}$

Another simpler feedback can also be used. This feedback does not use the parameter η which enables to smooth the rapid variations of the phase:

$$\omega^2_{PLL(k+1)} = \frac{1}{\Delta t_{k+1}}\Delta\hat{\phi}_{k|k} + \hat{\omega}_{k|k} + \frac{\Delta t_{k+1}}{2}.\hat{\alpha}_{k|k}$$

B. Static case parametrization

In the static case, the smoothing feedback using $\omega^1_{PLL(k+1)}$ is used. This feedback depends on η a smoothing parameter which enables to limit the reactivity of the feedback and thus stabilizes the loop filter. The tracking configuration of the improved receiver is presented in table 1.

TABLE I: TRACKING CONFIGURATIONS OF IMPROVED RECEIVER ADOPTED FOR SCINTILLATION IN THE STATIC CASE

	Nominal Scintillations	Intense Scintillations	Worst case Scintillations
Discri	atan2 + known nav bits	atan2 + known nav bits	atan2 + known nav bits
Bl (Hz)	10	10	3
Integration time (ms)	10	10	1
Etha (η)	0.77	0.77	0.96

C. Dynamic case parametrization

In the dynamic case, the feedback $\omega^2_{PLL(k+1)}$ is used. Contrary to the static case, parameter η is not used, because the dynamics of the receiver is too difficult to follow. This feedback allows a faster reaction to the strong variations of the control signal on contrary to the static case since the smoothing tuned by η is not used.

For nominal and intense scintillations, the discriminator used depends on the estimated value of C/N$_0$ and on the navigation data bit. Above 35dBHz, atan2 is used but only if the two methods for data bit estimation give the same result. In the contrary, atan is used.

TABLE II: TRACKING LOOP CONFIGURATIONS OF THE IMPROVED RECEIVER IN THE DYNAMIC CASE

	Nominal Scintillations	Intense Scintillations	Worst case Scintillations
Discri	atan2 if (C/N$_0$>35dBHz and $\hat{d}_1 = \hat{d}_2$) atan if C/N$_0$<35dBHz	atan2 if (C/N$_0$>35dBHz and $\hat{d}_1 = \hat{d}_2$) atan if C/N$_0$<35dBHz	atan
Bl (Hz)	10	10	3
Integration time (ms)	10	10	1
Etha (η)	X	X	X

V. SIMULATION

A. Simulation environment

This section describes the simulation environment used to model the scintillation phenomena, the GNSS signal processing modules (signal generation and reception architectures) and the classical GNSS signal tracking algorithm.

The simulator selected to run the simulations is the JGNSS simulator, owned by CNES. It models a GPS L1 C/A processing chain including: sample level GPS L1 C/A signal generation, propagation channel model including scintillation and multipath, GPS L1 C/A tracking.

Position calculation module is not run in this study that focuses on the robustness of the tracking loops.

Signal duration of 100 seconds was selected for the simulations. This duration is sufficiently long for the GNSS tracking loops to be disturbed by the scintillations and for the simulation time to remain acceptable (about 12h).

Two cases are considered:

- Static receiver (ground station)
- Dynamic receiver in an aircraft in approach. A straight line descent with a constant velocity of 70 m/s is considered.

The RF bandwidth will be assumed to be different between the static case (ground station) and dynamic case (aircraft in approach), for the simulations with the standard receiver or for the simulations with the enhanced receiver.

TABLE III: RECEIVER PARAMETERS

	Ground station	Aircraft
Sampling Frequency	100MHz	100MHz
Intermediate frequency Fi	4MHz	4MHz
RF/IF Bandwidth	8 MHz	2 MHz
Number of quantization bits in ADC	3 bits	3 bits

Furthermore, two values of C/N0 will be considered for the undisturbed direct path in case of static and dynamic receiver: a C/N0 of 45dBHz and a C/N0 of 35dBHz.

1) Conventionnal tracking loop parametrization

A comparison of performances between a conventional architecture and the Kalman algorithm is performed to observe the improvements.

The architecture of the standard receiver is classical. It is based on FLL-aided PLLs pushing the DLL using correlator outputs. The correlators and the loops are set with parameters having classical values (Bl=1 Hz for the DLL and Bl=10Hz for the FLL and PLL, Early minus Late chip-spacing =0.25). Integration time of 20 ms is used. The phase discriminator used in the classical architecture is of type ATAN.

2) Multipath model
a) Static case

The model proposed is the combination of two sub-models: the first part is a model of the parameters of the multipath; the second part is a model of the impact of this multipath on the pseudorange measurements.

The model of the parameters of the multipath is simplified mainly by drawing randomly these parameters. We propose to consider simultaneously 2 reflected rays at each epoch.

The 2 reflected rays considered are a ray reflected by the ground underneath the antenna, and a ray reflected by a random obstacle located around the antenna.

b) Dynamic case

In the dynamic case, the high resolution aeronautical model developed for the European Space Agency (ESA) in 2002 by Joanneum Research, University of Vigo and the DLR, based on measurements is used [12].

This model includes a direct, a refracted component, a strong fuselage echo changing very slowly, and a ground echo changing very rapidly. The outputs of this model are the relative delay, relative amplitude and relative carrier phase shift of the multipath relative to the direct signal.

3) Scintillation scenarios

Three scintillation scenarios were selected:

- A nominal scintillation scenario: it occurred on 23/10/2010, with a solar flux of 78 and S_4 of 0.3.
- An intense scintillation scenario: it occurred on 01/12/2006, with a solar flux of 84 and S_4 of 0.5.
- A worst case scintillation scenario: it occurred in october 2003. The solar flux reached a maximum of 279. The S_4 is set to 0.9.

B. GISM data simulated

CLS bought the GISM software from the company IEEA. This software provides the times series of the phase and amplitude fluctuations of the signals with a 50 Hz update rate as well as the scintillations parameters S_4 and sigma-phi for the different scenarios considered. These samples are interpolated in a linear way to bring them to the simulator sampling frequency of 100MHz.

Figure 2 to Figure 7 illustrate the phase and amplitude variations of the signal for the scintillation scenarios considered.

For the nominal case, it was chosen to consider the maximum intensity period of the simulated scintillations in the GISM file. This explains the presence of the C/N0 peak at -23dBHz on Figure 5. This peak corresponds to the maximum signal intensity variation for nominal scintillations with a solar flux of 78. It is a singular phenomenon which does not represent the classical phase variations for nominal perturbations, but it has been chosen to study the receiver behavior facing such a huge perturbation.

For the intense case, we can see on Figure 6 that power variations are larger compared to the normal scintillation case, except for the absence of a very deep C/N0 peak like in the nominal case. These data correspond to a solar flux of 84. We did not choose to consider the maximum case in this situation, so the variations considered are average variations for the intense scintillation case.

For the worst case scenario, Figure 4 shows the variations of the Doppler offset due to worst case scintillation generated by GISM. We can see that Doppler frequency variations generated by scintillations lie within -800 and +800Hz, meaning that the phase can evolve by 1600*0.02= 32 cycles in 0.02 seconds which is the integration time considered for the standard receiver.

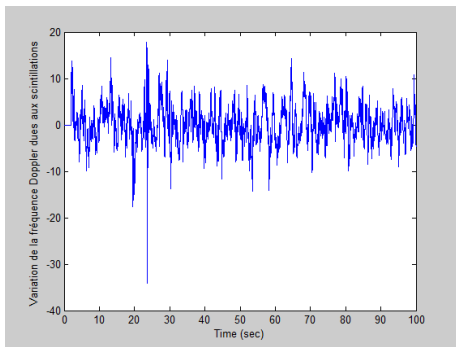Such a Doppler variation is extreme and results will not be good in such cases.

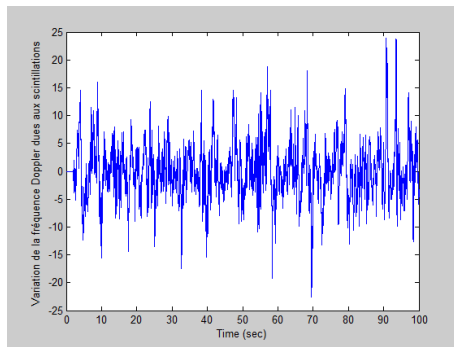Figure 2: Variations of the received signal Doppler offset in the nominal scintillation case

Figure 3: Variations of the received signal Doppler offset in the intense scintillation case
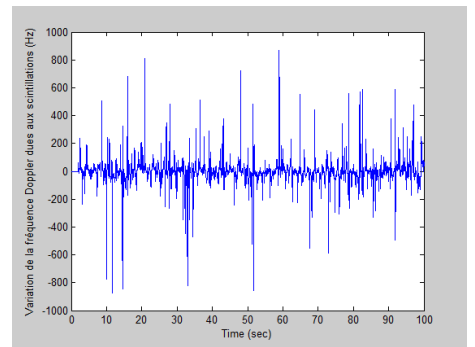

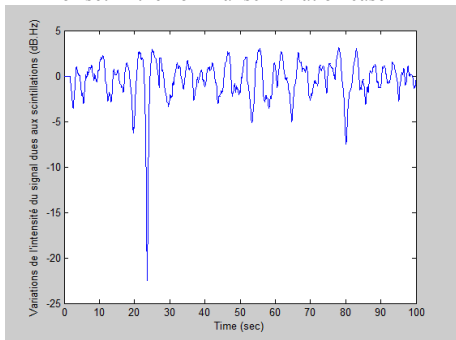Figure 4: Variations of the received signal Doppler offset in the worst scintillation case

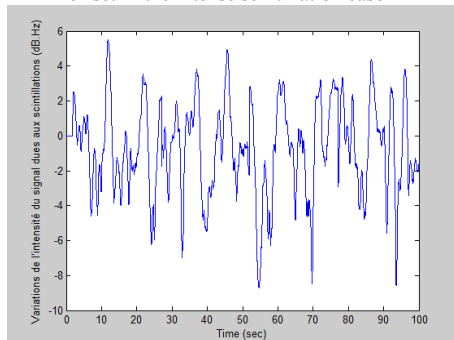Figure 5: Variations of the received signal power in the nominal scintillation case

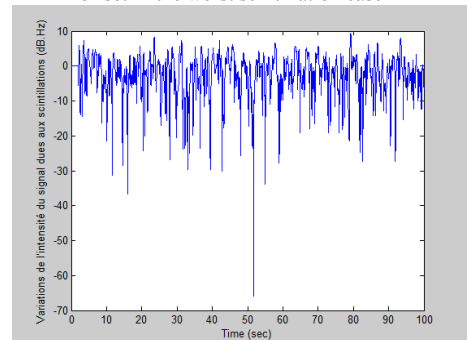Figure 6: Variations of received signal power in the intense scintillation case

Figure 7: Variations of received signal power in the worst scintillation case

C. Simulation results

We compare here the simulation results obtained with the standard receiver with the results obtained with the improved receiver in the static and dynamic cases.

1) Static case

The figures below present the performance obtained for the static receiver in the standard and improved version (KFP), with the loop filter replaced by a Kalman filter equivalent to a 3rd order filter for the three scintillation scenarios and for 2 signal powers.

Figure 9: Number of re-acquisition for standard receiver (blue colors, left and middle right sticks) and KFP receiver (red colors, middle left and right sticks) for the static case.
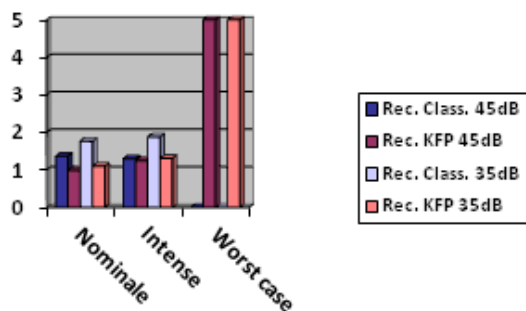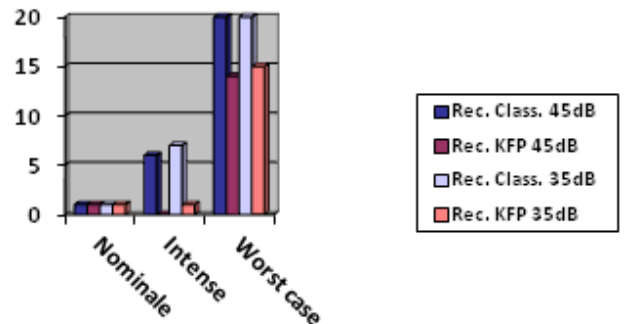

Figure 8: Standard deviation of phase tracking error (cm) for standard receiver (blue colors, left and middle right sticks) and KFP receiver (red colors; middle left and right sticks) for the static case.
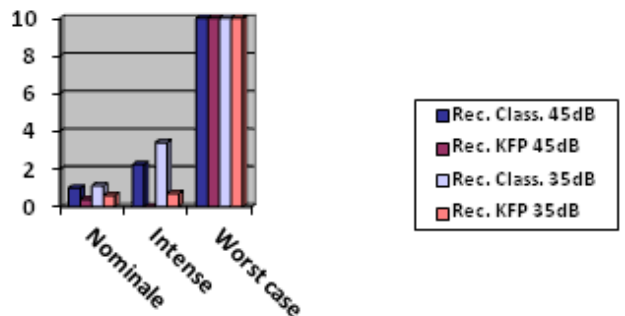

Figure 10: Percentage of loss of lock for standard receiver (blue colors, left and middle right sticks) and KFP receiver (red colors, middle left and right sticks) for the static case.

Figure 8, Figure 9 and Figure 10 present the better tracking performance of the KFP compared to conventional tracking. In the nominal and intense scintillation scenarios, the standard deviation of phase tracking error is lower for KFP compared to standard receiver.

KFP shows better results for these two scenarios when looking at the loss of lock rate too.

The number of re-acquisition tends to decrease too. For both signal power (35 and 45 dB.Hz) and for both algorithms (standard and KFP), only one re-acquisition is observed. This one cannot be overcome because of the scintillation pick at the 23th second of simulation. However, for the intense scenario, there are about 6 and 7 re-acquisitions for the standard receiver compared to 0 and 1 for the KFP with a power of 45dB.Hz and 35dB.Hz respectively.

In this worst case, the use of KFP with a narrow bandwidth (3Hz) and a large etha (0.96) has to be adopted because phase variations can reach 1.6 cycle/ms, which is too fast to be followed through 1 ms integration as the discriminator has an operating region of -0.5…+0.5 cycles.

This tuning allowed decreasing the number of re-acquisitions compared to the FPLL case, and a phase tracking error standard deviation could be estimated. However, the large value of these standard deviations at 35 and 45 dBHz on Figure 8 (cut to 5cm for scaling matter) show that the phase is not properly tracked as we can see on the loss of lock rate on Figure 10 (cut to 10% for scaling matter).

Tracking with the FPLL leads to too many re-acquisitions over the 100s simulation time to be able to estimate a valid phase tracking error standard deviation.

Indeed, the number of re-acquisitions is about 80 on the simulation duration. For a matter of scale, it has been cut at 20 on Figure 9. The number of re-acquisitions is highly reduced by using the KFP, except in the nominal case where the singular power loss of 23dB cannot be overcome.

1) Dynamic case

The figures below present the performance obtained for the dynamic receiver in the standard and KFP version, for the 3 scintillation scenarios and for 2 signal powers.
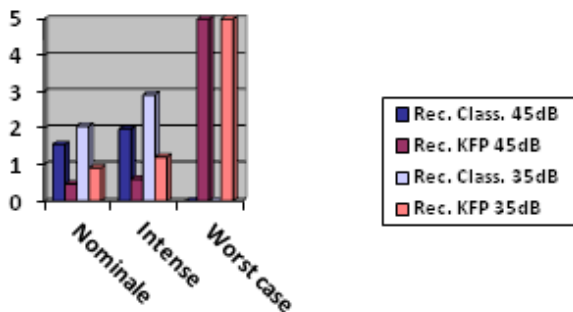

Figure 11: Standard deviation of phase tracking error (cm) for standard receiver (blue colors, left and middle right sticks) and KFP receiver (red colors; middle left and right sticks) for the dynamic case.
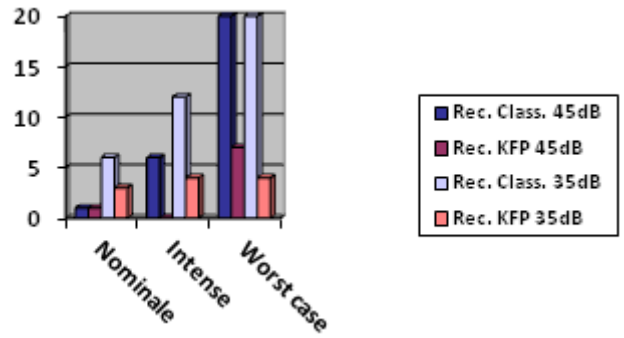

Figure 12: Number of re-acquisition for standard receiver (blue colors, left and middle right sticks) and KFP receiver (red colors, middle left and right sticks) for the dynamic case.
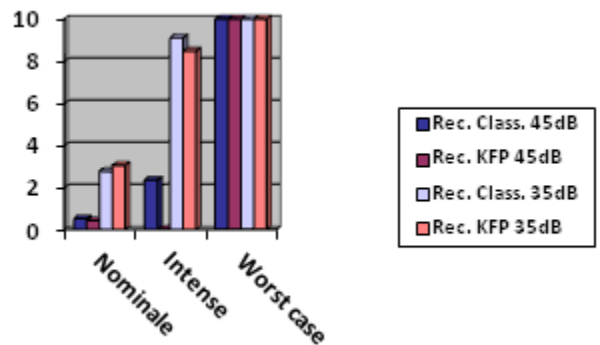

Figure 13: Percentage of loss of lock for standard receiver (blue colors, left and middle right sticks) and KFP receiver (red colors, middle left and right sticks) for the dynamic case.

The estimated standard deviations of the phase tracking errors are lower for the KFP than for the FPLL in the nominal and intense cases.

In the worst scintillation case, the standard deviation of the phase tracking error is again large, showing that the phase is not tracked accurately.

As for the static case, the number of re-acquisitions is again low compared to the conventional tracking configuration, except for the nominal scintillation case.

It can also be noted that at 35dBHz for the nominal and intense scintillation, even though the number of re-acquisitions is lower when using the KFP, the loss of lock rate did not decrease. This is due to the fact that the receiver takes more time to achieve bit synchronization after a re-acquisition and stays in a DLL + FLL mode.

In the worst scintillation case, the rate of loss of lock at 45dBHz goes from 37% for the classical dynamic receiver to 27% for the improved dynamic receiver. These statistics cannot be seen on the Figure 13 because it has been cut to 10% for scaling matter.

The receiver dynamics sometimes creates problems for re-acquisitions and can lead to false peak detections, leading in turn to new re-acquisitions until a meaningful peak is found. Moreover, the change of discriminator (atan2 for C/N0>35dB.Hz and atan if C/N0<35dB.Hz) appeared to be

not really usefull. Results would have been pretty much the same if we used the atan discriminator for the whole C/N0 range. Indeed, in case of phase tracking error higher than 90°, some error occurred when demodulating the navigation data bits and the receiver lost tracking as in case of atan. Complementary results about this study can be found in [1].

VI. CONCLUSION AND FUTURE WORK

In this study, it was observed that standard tracking was quite robust for nominal scintillations, but often lost lock in more severe situations. We analyzed the Kalman Filter PLL (KFP) algorithm and proposed improvements to this technique. We observed that the KFP improved carrier tracking in all situations.

In the future stages of the study, we can propose the following options for further improvement. First of all, a way to adapt the loop bandwidth as a function of detected scintillation intensity could be tested. Acceleration input could also be used for tracking loops. It could also be analyzed a way to replace the classical DLL by more robust DLL to improve tracking during strong perturbations. Finally, a frequency discriminator could be added as an additional Kalman filter observable input to maintain carrier tracking even if the phase is not tracked.

The proposed algorithms are going to be tested with real scintillation data, collected by CNES, the French space agency, in collaboration with ASECNA, the African civil aviation agency. A network of 5 receivers will be deployed in early 2013 in equatorial Africa, as shown in Figure 14. At two of these sites, Dakar and Lome, ISM and signal digitizers will also be deployed in order to digitize signals in presence of scintillations. This data collection will permit to validate our algorithm performances on real data and to evaluate the representativity of the scintillation time series generated with GISM.

Figure 14: location of the scintillation data collection network deployed by CNES and ASECNA in 2013.

REFERENCES

[1] C. Macabiau, V. Barreau, J.J. Valette, G. Artaud, L. Ries, "Kalman Filter Based Robust GNSS Signal Tracking Algorithm in Presence of Ionospheric Scintillations", ION GNSS 2012, in press.

[2] Y. Beniguel, "GISM user manual", 2010.

[3] G. Bishop, S. Basu, K. Groves, Phillips. "Upcoming Ionospheric Impacts on GPS at Solar Max What Do We Know/What Do We Need?", ION GPS 1996.

[4] P. Doherty, S. Delay, C. Vallardes, J. Klobuchar, "Ionospheric Scintillation Effects in the Equatorial and Auroral Regions", ION GNSS 2000, Salt Lake City, Utah, 662–671, 2000.

[5] P. Henkel, K. Giger and C. Günther, "Multi-Carrier Vector Phase Locked loop for Robust Carrier Tracking ". In: Proc. of European Navigation Conference (ENC), 2008-25-04, Toulouse, France.

[6] P. Kintner, T. H Humphreys, J. Hinks, "GNSS and Ionospheric Scintillation: How to survive the next solar maximum", Inside GNSS, July/August 2009.

[7] Kondo, S., T. Ebinuma, N. Kubo, and A. Yasuda, "Evaluation of tracking performance in the presence of ionosphere scintillation on GPS signal in Japan," Proc. ION GNSS, pp.2832-2839, Ft. Worth, TX, Sept. 2007.

[8] P. Lassudrie Duchesne, Y. Beniguel, A. Bourdillon, R. Fleury, J-J. Valette, Minh Le Huy, L. Tran Thi, "Les effets de la scintillation ionosphérique sur le GPS", july 2010, vol. 58, n° 231, pp. 17-34, 2010.

[9] F. Legrand, Thesis (2002): "Modèle de boucle de poursuite de signaux à spectre étalé et méthode d'amélioration de la précision des mesures brutes », 2002.

[10] M. Psiaki, T. Humphreys, A. C Cerruti, S. Powell, P. Kintner, "Tracking L1 C/A and L2C signals through ionospheric scintillations", ION GNSS 2007.

[11] S. Radicella, "The NeQuick model genesis, uses and evolution", Annals of Geophysics, vol 52, N° 3-4, 2009.

[12] A. Steingass, A. Lehner, F. Perez-Fontan, E. Kubista, M. Jesus Martin and B. Arbesser-Rastburg, "The High Resolution Aeronautical Multipath Navigation Channel", ION GPS 2004.

[13] J. Tian, L. Yang, B. Hang, "A Novel GNSS Weak Signal Acquisition Using Wavelet Denoising Method", Proceedings of the NTM ION 2008.

[14] F. Van Graas, A. Soloviev, M. U. de Haag, and S. Gunawardena, "Closed-Loop Sequential Signal Processing and Open-Loop Batch Processing Approaches for GNSS Receiver Design", IEEE Journal of Selected Topics in Signal Processing, Vol. 3, No. 4, 2009.

[15] L. Zhang, Y. Morton, "Tracking GPS Signals under Ionosphere Scintillation Conditions", ION GNSS 2009.

[16] L. Zhang, Y. Morton, F. Van Grass, T. Beach, "Characterization of GNSS signal parameters under ionosphere scintillation conditions using software based tracking algorithms," Proc. ION/IEEE PLANS 2010.